Observation of Two-Mode Squeezing in the Microwave Frequency Domain

C. Eichler, D. Bozyigit, C. Lang, M. Baur, L. Steffen, J. M. Fink, S. Filipp, and A. Wallraff

Department of Physics, ETH Zürich, CH-8093, Zürich, Switzerland

(Received 24 January 2011; revised manuscript received 8 June 2011; published 6 September 2011)

Continuous variable entanglement between two modes of a radiation field is usually studied at optical frequencies. Here we demonstrate experiments that show the entanglement between microwave photons of different energy in a broadband squeezed beam. We use a Josephson parametric amplifier to generate the two-mode correlated state and detect all four quadrature components simultaneously in a two-channel heterodyne setup using amplitude detectors. Analyzing two-dimensional phase space histograms for all possible pairs of quadratures allows us to determine the full covariance matrix, which is in good agreement with the one expected for a two-mode squeezed state.

DOI: 10.1103/PhysRevLett.107.113601 PACS numbers: 42.50.Pq, 03.67.Lx, 42.50.Dv, 42.50.Lc

State tomography for more than a single mode of a radiation field allows us to characterize photon sources that display entanglement between propagating photons. At optical frequencies, well-established multimode state reconstruction techniques based on single photon counters exist. These have already allowed for a variety of experiments that demonstrated entanglement and the EPR paradox for continuous variables states [1–5]. A well-known representative for the class of optical entangled states is the two-mode squeezed vacuum [6], which has been used as a resource for continuous variable quantum computation, cryptography, and teleportation experiments [7–9].

In the microwave domain, state tomography experiments have recently been realized for single itinerant field modes [10–12]. In addition, multimode state reconstruction for intracavity fields of two spatially separated cavities has been demonstrated [13]. Here we present heterodyne state tomography techniques that allow for the state reconstruction of two itinerant modes. We apply these techniques to reconstruct the covariance matrix of a two-mode squeezed state generated in a Josephson parametric amplifier.

Noise squeezing at microwave frequencies has been demonstrated for these amplifiers in the degenerate [14] as well as in the nondegenerate case of parametric amplification [15]. The general interest in parametric amplification [16,17] has steadily grown in the recent past [14,18,19], because it allows for investigating the quantum properties of microwave radiation [20], superconducting qubits [21], and nanomechanical oscillators [22] at high signal-to-noise ratios.

In this Letter, we present experimental state tomography for two output field modes of a parametric amplifier which generates entangled photon pairs of frequencies $\omega_1/2\pi$ and $\omega_2/2\pi$ from the input vacuum noise by annihilating two pump photons $2\omega_p = \omega_1 + \omega_2$. The corresponding field modes a_1 and a_2 emitted from the single broadband resonator mode, which are separated in frequency space [23,24], are described by a two-mode squeezed state. Alternatively, one can analyze squeezing correlations between two spatially separated modes by sending two squeezed states through a balanced beam splitter [11] or by using two parametrically coupled resonators with different output ports [15]. Here, we first describe the measurement setup, discuss the device parameters, and characterize the system as a phase-preserving amplifier. We then measure the covariance matrix and reconstruct the Gaussian Wigner function of the four quadrature components [7].

Our parametric amplifier (Fig. 1) is realized as a $\lambda/4$ transmission line resonator terminated by an array of three superconducting quantum interference devices (SQUIDs) [25]. The fundamental mode of the resonator is in good approximation described as a nonlinear oscillator with an effective Hamiltonian

$$H = \hbar\omega_r a^\dagger a + \hbar\frac{K}{2} a^\dagger a^\dagger a a, \tag{1}$$

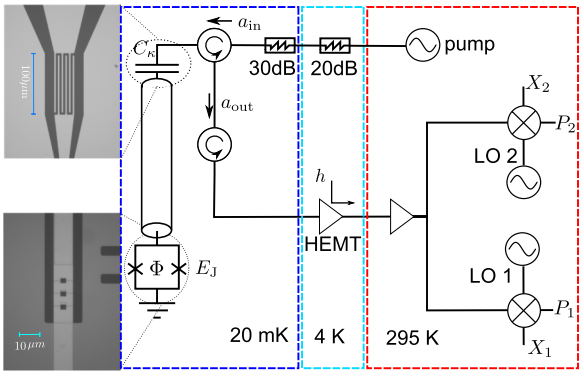

FIG. 1 (color online). Schematic of the experimental setup. The input and output modes of the parametric amplifier are separated by using a circulator. Input modes a_{in} are in the vacuum state due to cold attenuators. The output signal is amplified by a cold HEMT amplifier at 4 K, introducing the dominant part of additional system noise h. Mixing with two individual local oscillators at room temperature allows for a simultaneous detection of two distinct modes in frequency space.

where the nonlinearity is provided by the SQUIDs. The Kerr constant K as well as the resonator frequency $\omega_r/2\pi$ are functions of the effective Josephson energy E_J of the SQUID array [26]. Thus, by changing the flux bias ϕ through the SQUID loops, the resonator frequency and the Kerr constant can be tuned. A measurement of the flux-dependent resonance frequency allows us to extract both the effective Josephson energy and the Kerr constant. Fitting the data shown in Fig. 2(a) to a model described in Ref. [26] leads to the approximate values $E_{J,\max}/h \approx 1.3$ THz and $K/\omega_{r,\max} = -1.1 \times 10^{-6}$ at the maximum resonance frequency where $\omega_{r,\max}/2\pi \approx 6.4$ GHz. To further characterize the resonator, we have measured the reflection coefficient Γ in the linear regime [Fig. 2(b)]. From the real and imaginary parts of Γ, we can extract the coupling of the resonator to the transmission line $\kappa/2\pi \approx 15$ MHz, which dominates over the internal loss $\gamma_i/2\pi \approx 2.5$ MHz.

If a nonlinear oscillator is pumped close to its bifurcation point with a coherent pump tone at frequency $\omega_p/2\pi$, the relation between input and output field modes $a_{\text{in}}(\Delta)$ and $a_{\text{out}}(\Delta)$, respectively, can be written as [27]

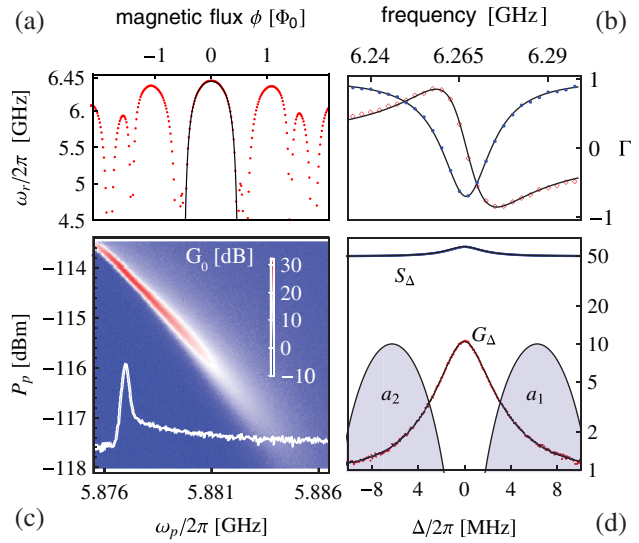

FIG. 2 (color online). (a) Measured (dots) and calculated (solid line) resonance frequency $\omega_r/2\pi$ vs magnetic flux ϕ. (b) Measured real (blue dots) and imaginary (red diamonds) parts of the reflection coefficient Γ in the linear regime for magnetic flux $\phi = 0.23$ and fit to theory (lines). (c) Measured maximum gain G_0 as a function of pump frequency $\omega_p/2\pi$ and pump power P_p. A horizontal cut through the data at $P_p \approx -114$ dBm is shown in white. (d) Measured gain G_Δ (red dots) and power spectral density S_Δ (blue dots) for a fixed pump tone as a function of detuning Δ. The 3 dB bandwidth of the gain curve with a maximum gain of 10 dB is $B/2\pi \approx 3.6$ MHz. The absolute values of the sinc Chebyshev filter functions $f_1(\Delta)$ and $f_2(\Delta)$, defining modes a_1 and a_2, are shown on a logarithmic scale (arbitrary units) as the lines enclosing the shaded areas.

$$a_{\text{out}}(\Delta) = A_\Delta a_{\text{in}}(\Delta) + B_\Delta a_{\text{in}}^\dagger(-\Delta). \quad (2)$$

Here Δ is the detuning from the pump frequency $\omega_p/2\pi$, where $\Delta > 0$ ($\Delta < 0$) corresponds to frequency components at the upper (lower) sideband of the pump. The frequency-dependent coefficients A_Δ and B_Δ fulfill the relation $|A_\Delta|^2 - |B_\Delta|^2 = 1$. Thus Eq. (2) describes a minimal form quantum linear amplifier with gain $G_\Delta = |A_\Delta|^2$ [17]. When a signal is applied at one sideband, the frequency components of the other sideband are usually called idler modes. The device acts as a phase-preserving amplifier when only the signal modes are analyzed at its output.

We have characterized our device as such an amplifier. To measure the maximum gain G_0 as a function of $\omega_p/2\pi$ and pump power P_p, we apply an additional weak coherent tone ($P_s \approx -170$ dBm) with a small detuning of $\Delta/2\pi = 2.5$ kHz to the input port. We measure the reflected amplitude at this frequency and compare the result with the one that we obtain when the pump tone is turned off. The absolute square of this ratio is the gain G_0; see Fig. 2(c). We identify the critical point where G_0 takes its largest value [28] at $\omega_{p,\text{crit}}/2\pi \approx 5.877$ GHz and $P_{p,\text{crit}} \approx -114$ dBm. For pump powers below $P_{p,\text{crit}}$, we are in the stable amplifier regime. A decrease in pump power leads to smaller gain but to larger amplifier bandwidth B. The gain-bandwidth product remains constant according to the relation $\sqrt{G_0}B \propto \kappa$ [27], which we have verified experimentally.

For the following measurements, we have fixed the coherent pump at $\omega_p/2\pi = 5.882\,75$ GHz and $P_p \approx -116.9$ dBm. The signal frequency dependence of the gain G_Δ for this pump tone is shown in Fig. 2(d). We have also measured the noise power spectral density S_Δ [29], which can be decomposed into two contributions:

$$S_\Delta \delta(\Delta - \Delta') = \langle h^\dagger(\Delta') h(\Delta)\rangle + \langle a_{\text{out}}(\Delta') a_{\text{out}}^\dagger(\Delta)\rangle. \quad (3)$$

The first term on the right-hand side describes the system noise part, which is dominated by the high-electron-mobility transistor (HEMT) amplifier noise. In the relevant range it is almost frequency-independent and leads to a constant contribution of $N_{\text{noise}} \approx 48$ noise photons to S_Δ [Fig. 2(d)]. The second term in Eq. (3) stands for the noise at the output of the parametric amplifier. Since it can be interpreted as the amplified vacuum noise, the curves for G_Δ and $(S_\Delta - N_{\text{noise}})$ are expected to be identical, which allows us to determine the system noise offset N_{noise}. Both data sets are well described by the same theoretical curve [27]; see the black lines in Fig. 2(d).

Up to now, we have characterized our device as a phase-preserving amplifier. If the input of the parametric amplifier is in the vacuum, the output is amplified vacuum noise. However, due to the parametric nature of this amplification process, where signal and idler photons are always generated in pairs, we expect the signal and idler frequency noise

to be strongly correlated. More specifically, the signal and idler output modes should approximately be described by a two-mode squeezed vacuum state. We verify this experimentally by pumping the resonator with the same coherent pump tone as before and recording the quadrature amplitudes in both modes individually.

The resonator output is amplified with the same HEMT amplifier as used for the gain measurements and split into two channels. To separate signal and idler frequency components from each other (Fig. 1), we effectively downconvert the microwaves in both channels by mixing them with local oscillator tones at frequencies $\omega_{\mathrm{LO1}}/2\pi$ and $\omega_{\mathrm{LO2}}/2\pi$ set 6.25 MHz above and below the pump frequency, respectively. The voltages are digitized every 10 ns with an analog to digital converter. By using a field programmable gate array, the data are digitally filtered with a sinc Chebyshev filter function $f(\Delta)$ as shown in Fig. 2(d). As a result, the two detection channels linearly detect photons with frequencies in the windows $f_1(\Delta) = f(\Delta - 2\pi \times 6.25\ \mathrm{MHz})$ and $f_2(\Delta) = f(\Delta + 2\pi \times 6.25\ \mathrm{MHz})$, respectively. The filter is designed such that both $f_1(0) = f_2(0) = 0$, rejecting the coherent pump tone.

As a result, the four quadrature components that we extract after the digital data processing correspond to measurement results of the complex valued operators [30]

$$\hat{X}_{1,2} + i\hat{P}_{1,2} \equiv a_{1,2} + h_{1,2}^{\dagger} \tag{4}$$

with $a_{1,2} = \int_{-\infty}^{\infty} d\Delta f_{1,2}(\Delta) a_{\mathrm{out}}(\Delta)$ and $h_{1,2}$ equivalently. a_1 and a_2 describe a pair of signal and idler modes at the parametric amplifier output. The system noise modes h_1 and h_2 are in thermal states with mean photon number N_{noise}. We have verified this by measuring 2D quadrature histograms for the noise modes while turning off the pump tone where we observe perfectly circular symmetric Gaussian distributions [10]; see Fig. 3(a).

According to Eq. (2), we expect a_1 and a_2 to be approximately in a two-mode squeezed vacuum state $\exp\{r a_1 a_2 - r a_1^{\dagger} a_2^{\dagger}\}|00\rangle$ [7]. The relative phase between the two local oscillators has been chosen such that the squeezing parameter r is real and related to the average gain by $\cosh^2(r) \approx \int_{-\infty}^{\infty} d\Delta |f_1(\Delta)|^2 G_{\Delta}$. The two-mode squeezed state is characterized by the covariances of the 4 quadrature components $\hat{\xi}_i \in \{\hat{x}_1, \hat{p}_1, \hat{x}_2, \hat{p}_2\}$ of the two modes, defined by $a_{1,2} = \hat{x}_{1,2} + i\hat{p}_{1,2}$. Quantum correlations for this state become most apparent in the relative "position" $\hat{x}_1 - \hat{x}_2$ and the total "momentum" $\hat{p}_1 + \hat{p}_2$ variables, which are squeezed below the standard vacuum limit 1/2 according to $\langle(\hat{x}_1 - \hat{x}_2)^2\rangle = \langle(\hat{p}_1 + \hat{p}_2)^2\rangle = e^{-2r}/2$, while each component itself is amplified $\langle\hat{\xi}_i^2\rangle = \cosh(2r)/4$. Since the two-mode squeezed state belongs to the class of Gaussian states, its Wigner function can be written as a multivariate normal distribution [7]

$$W(\alpha) = \frac{1}{4\pi^2\sqrt{\det \mathbf{V}}} \exp\left\{-\frac{1}{2}\alpha \mathbf{V}^{-1} \alpha^T\right\} \tag{5}$$

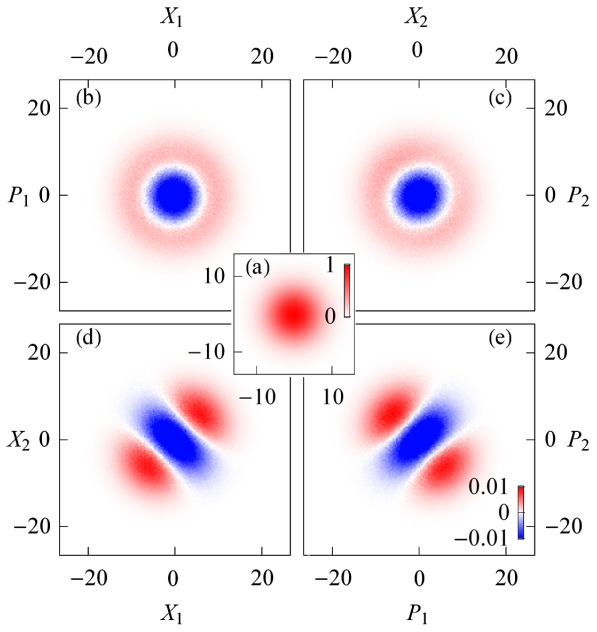

FIG. 3 (color online). (a) Quadrature histogram $\{X_1, P_1\}$ when the pump tone is turned off given in units of its maximal value. (b)–(e) Difference between quadrature histograms with the pump tone turned on and off for 4 different quadrature pairs in the same units as (a).

with the vector of quadrature components $\alpha = (x_1, p_1, x_2, p_2)$ and the quadrature covariance matrix $\mathbf{V}$ with elements $V_{i,j} = \langle\hat{\xi}_i\hat{\xi}_j + \hat{\xi}_j\hat{\xi}_i\rangle/2$ [7]. The two-mode phase space distribution is thus fully determined by the 4×4 covariance matrix $\mathbf{V}$, which describes the joint statistics of the amplitude fluctuations of the two modes.

To determine the elements of this matrix, we detect the four quadrature components as explained above [Eq. (4)] and store the results in two-dimensional histograms for the six possible pairs $\{X_1, P_1\}$, $\{X_2, P_2\}$, $\{X_1, P_2\}$, $\{X_2, P_1\}$, $\{X_1, X_2\}$, and $\{P_1, P_2\}$. For each pair, we first acquire a reference histogram with the pump turned *off* [Fig. 3(a)], which characterizes the quadrature distribution of the effective noise modes $h_{1,2}$, and a second histogram with the pump turned *on*. The differences between such histogram pairs (see Fig. 3) show a systematic change in the detected quadrature statistics when the resonator output in modes $a_{1,2}$ changes from the vacuum state to the state which is to be characterized. For the single-mode histograms $\{X_1, P_1\}$ and $\{X_2, P_2\}$, we observe a phase-independent increase in the quadrature fluctuations, reflected in the higher probability of measuring larger quadrature values [Figs. 3(b) and 3(c)]. Since the increase in fluctuations is circular symmetric, it corresponds to a phase-preserving amplification in each of the individual modes a_1 and a_2. However, for the cross-histograms $\{X_1, X_2\}$ and $\{P_1, P_2\}$, we find an increase in the fluctuations along one diagonal axes, indicated by the positive valued regions in the histogram differences [Figs. 3(d) and 3(e)], and a decrease in the other direction.

Both these observed features are characteristic for a two-mode squeezed state.

The measured data are further analyzed by separating the contributions of noise modes $h_{1,2}$ from those of modes $a_{1,2}$. We calculate all possible expectation values $\langle \hat{X}_i \hat{X}_j \rangle_{\text{on,off}}$ and $\langle \hat{X}_i \hat{P}_j \rangle_{\text{on,off}}$ from the 12 measured pump on and off histograms. Using relations such as $\langle \hat{x}_1^2 \rangle = \langle \hat{X}_1^2 \rangle_{\text{on}} - \langle \hat{X}_1^2 \rangle_{\text{off}} + 1/4$, which follow from Eq. (4), we can determine all second-order expectation values $V_{i,j}$. Related experiments have recently shown [10] that this separation of signal and noise moments can be reliably realized up to fourth order for single-mode histograms.

The result for the covariance matrix is shown in Fig. 4(a). Its diagonal elements express the amplified individual quadrature fluctuations in both modes. Their values are in good agreement with what we expect from the measured gain averaged over the filter function. The nonvanishing off-diagonal elements describe the squeezing correlations between the two modes and are important to demonstrate that the signal and idler photons are entangled. As a criterion for nonclassicality, we determine the total momentum fluctuations $\langle (\hat{p}_1 + \hat{p}_2)^2 \rangle$ and the relative position fluctuations $\langle (\hat{x}_1 - \hat{x}_2)^2 \rangle$, where we find both values squeezed below the standard quantum limit by -2.25 ± 0.16 and -1.89 ± 0.13 dB, respectively. In addition, we have verified that our measured covariance matrix fulfills the nonseparability criterion formulated in Ref. [31].

We have further checked the influence of finite thermal fluctuations on the presented results. In independent experiments [32] we have found $\bar{n} \approx 0.05$ as an upper bound for the thermal noise photon number at the input of the resonator. Evaluating our measurement data, taking this amount of thermal fluctuations into account, results in a reduction of the vacuum squeezing by only 10%. The amount of squeezing, that we have reached after optimizing the pump parameters, is limited by (i) the minimal filter bandwidth that can be implemented to detect the photons, (ii) the uncorrelated noise added by the parametric amplifier due to internal losses, and (iii) the phase stability that restricts us to operate the parametric amplifier at a point where it has relatively small gain [14].

We evaluate Eq. (5) to reconstruct the four-dimensional Wigner function $W(\alpha)$ for the two modes. In Figs. 4(b) and 4(d), we show a selection of characteristic projections of $W(\alpha)$ on two-dimensional subspaces. The $\{x_1, p_1\}$ projection, which describes the individual state of mode a_1, is amplified vacuum as expected. Compared to the theoretical vacuum Wigner function [Fig. 4(c)], it has a larger variance, indicating the phase-preserving amplification of vacuum noise. The $\{x_1, x_2\}$ projection is squeezed along the diagonal axis, visualizing the two-mode squeezing correlations between a_1 and a_2.

In summary, we have measured the full quadrature covariance matrix of a two-mode squeezed state and observed a reduction of quadrature noise in the variables

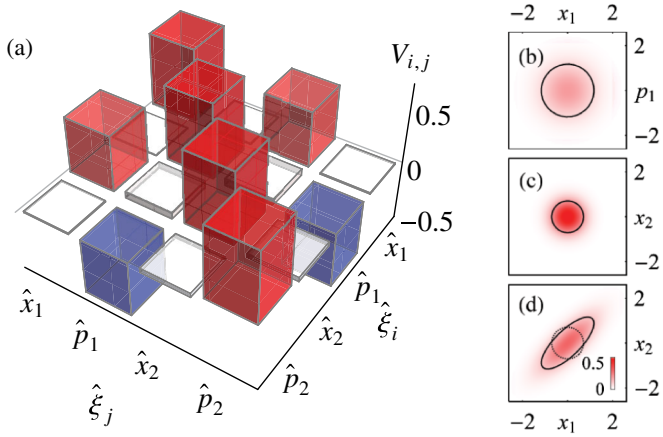

FIG. 4 (color online). (a) Measured quadrature covariance matrix $\mathbf{V}$ of the two-mode squeezed state which allows us to reconstruct the four-dimensional Wigner function. (b) and (d) show projections of this function onto two-dimensional subspaces with ellipses indicating where they drop to $1/e$ of their respective maximal value. (c) For comparison, we show the theoretical Wigner function of a vacuum state and its $1/e$ drop as a dashed circle also in (d).

$\hat{x}_1 - \hat{x}_2$ and $\hat{p}_1 + \hat{p}_2$ by approximately -2 dB below the standard quantum limit. We believe that this value can be increased by realizing a parametric amplifier with larger bandwidth, which furthermore allows for using the device as a low noise amplifier in other circuit QED experiments [21]. An important step towards future continuous variable quantum computation with propagating microwave photons [7] could be a combination of parametric amplifiers with beam splitters to spatially separate signal and idler modes and create nonlocal entanglement.

The authors acknowledge fruitful discussions with Barry Sanders, Konrad Lehnert, and Michel Devoret. This work was supported by the European Research Council (ERC) through a Starting grant and by ETHZ. S. F. acknowledges the Austrian Science Foundation (FWF) for support.

[1] A. Einstein, B. Podolsky, and N. Rosen, Phys. Rev. **47**, 777 (1935).
[2] M. D. Reid and P. D. Drummond, Phys. Rev. Lett. **60**, 2731 (1988).
[3] Z. Y. Ou, S. F. Pereira, H. J. Kimble, and K. C. Peng, Phys. Rev. Lett. **68**, 3663 (1992).
[4] S. A. Babichev, J. Appel, and A. I. Lvovsky, Phys. Rev. Lett. **92**, 193601 (2004).
[5] M. Vasilyev, S.-K. Choi, P. Kumar, and G. M. D'Ariano, Phys. Rev. Lett. **84**, 2354 (2000).
[6] R. Loudon and P. L. Knight, J. Mod. Opt. **34**, 709 (1987).
[7] S. L. Braunstein and P. van Loock, Rev. Mod. Phys. **77**, 513 (2005).
[8] A. Grosshans *et al.*, Nature (London) **421**, 238 (2003).
[9] A. Furusawa *et al.*, Science **282**, 706 (1998).
[10] C. Eichler *et al.*, Phys. Rev. Lett. **106**, 220503 (2011).

[11] F. Mallet *et al.*, Phys. Rev. Lett. **106**, 220502 (2011).
[12] E. P. Menzel *et al.*, Phys. Rev. Lett. **105**, 100401 (2010).
[13] H. Wang *et al.*, Phys. Rev. Lett. **106**, 060401 (2011).
[14] M. A. Castellanos-Beltran *et al.*, Nature Phys. **4**, 929 (2008).
[15] N. Bergeal, F. Schackert, L. Frunzio, and M. H. Devoret, arXiv:1011.4000v1.
[16] B. Yurke and J. S. Denker, Phys. Rev. A **29**, 1419 (1984).
[17] C. M. Caves, Phys. Rev. D **26**, 1817 (1982).
[18] N. Bergeal *et al.*, Nature (London) **465**, 64 (2010).
[19] E. A. Tholen *et al.*, Phys. Scr. **T137**, 014019 (2009).
[20] F. Mallet *et al.*, Nature Phys. **5**, 791 (2009).
[21] R. Vijay, D. H. Slichter, and I. Siddiqi, Phys. Rev. Lett. **106**, 110502 (2011).
[22] J. D. Teufel *et al.*, Nature Nanotech. **4**, 820 (2009).
[23] H. Yonezawa, S. L. Braunstein, and A. Furusawa, Phys. Rev. Lett. **99**, 110503 (2007).
[24] A. Kamal, A. Marblestone, and M. Devoret, Phys. Rev. B **79**, 184301 (2009).
[25] M. Sandberg *et al.*, Appl. Phys. Lett. **92**, 203501 (2008).
[26] M. Wallquist, V. S. Shumeiko, and G. Wendin, Phys. Rev. B **74**, 224506 (2006).
[27] B. Yurke and E. Buks, J. Lightwave Technol. **24**, 5054 (2006).
[28] R. Vijay, M. H. Devoret, and I. Siddiqi, Rev. Sci. Instrum. **80**, 111101 (2009).
[29] C. Lang *et al.*, Phys. Rev. Lett. **106**, 243601 (2011).
[30] M. P. da Silva, D. Bozyigit, A. Wallraff, and A. Blais, Phys. Rev. A **82**, 043804 (2010).
[31] R. Simon, Phys. Rev. Lett. **84**, 2726 (2000).
[32] J. M. Fink *et al.*, Phys. Rev. Lett. **105**, 163601 (2010).